Primary study on the efficiency of the discrete generalized multigroup method Based on proper orthogonal decomposition

ZHANG Qian[a*], WU Shifu[b], ZHANG Jinchao[b]
[a] *Laboratory for Advanced Nuclear Energy Theory and Applications, Zhejiang Institute of Modern Physics, Department of Physics, Zhejiang University, Hangzhou, Zhejiang 310058, China*
[b] *Fundamental Science on Nuclear Safety and Simulation Technology Laboratory, Harbin Engineering University, Harbin 150001, China*
[*] *Corresponding author: zhangqian0515@zju.edu.cn*

Abstract: In this article, we explore the efficiency of the discrete generalized multigroup (DGM) method, underpinned by the proper orthogonal decomposition (POD). The DGM method can utilize orthogonal basis functions to collapse fine-group fluxes and cross sections to a coarse-group structure. By solving the neutron transport equation in a coarse-group structure, the DGM method can effectively reconstruct fine-group flux. To study the effectiveness and the efficiency of this method, we choose two typical benchmark problem, includes: 1D UO_2-MOX-combination assembly problem and 1D HTTR assembly problem. We analyze the accuracy of the method based on different snapshot and the efficiency improvement by limiting the truncation order and reconstruction iterations is further studied. By constraining reconstruction iterations, this method can reconstruct fine-group energy spectrum with the majority of fine-group flux deviations within 1%, while utilizing only 40% of the time required for fine-group transport calculation.

***Keywords :** the discrete generalized multigroup method; proper orthogonal decomposition; interference; cross section collapsing; efficiency*

1. Introduction

In the field of reactor physics design, the deterministic two-step method remains the primary simulation method, due to the advancement of one-step methods with the limitations in computational resources. However, the current two-step method is based on equivalent homogenization and full reflection boundary assembly calculations, which can't effectively meet the demands of increasingly complex designs for the new-generation reactor cores [1]. Various approaches have been explored to address the shortcomings of the existing two-step method framework [2]. Among these approaches, one method is the discrete generalized multigroup method (DGM), which uses an orthogonal basis to convert a set of fine-group cross sections into a set of cross section moments mapped to a coarse-group structure [3-5]. These coarse-group cross section moments may be used as cross sections in coarse-group transport calculations, which lead to coarse-group flux moments. The coarse-group flux moments can be expanded to produce the fine-group flux using the basis functions. This fine-group flux can be used to reconvert the fine group cross sections to coarse group moments, which continues iteratively until convergence to eliminates the error from hypothetical fine energy spectrum[6]. However, this method needs to solve the higher order moments to obtain sufficiently approximate flux spectrum[7]. Richard Reed further developed this method by introducing proper orthogonal decomposition (POD) into this field. performing POD on energy spectrum snapshots can obtain orthogonal basis functions that contain physical information, which can effectively reduce the truncation order[7-9]. However, these studies were limited to problems related to light water reactors and didn't extensively investigate efficiency. In this work, our research expands this method to the more complex energy spectrum of the High-Temperature Test Reactor (HTTR) problem and conducts preliminary efficiency studies.

2. Background

In this section some of the techniques used to model the detector channel are described. The channel model includes a SiC detector, cable, preamplifier, amplifier, and discriminator models.

2.1 Detector Model

Zhu and Forget developed the discrete generalized multigroup(DGM) method, which is a way to represent the energy-space of a problem from within most transport approximations[4]. In this study, we use discrete ordinates as this this approximation. Due to it, we start with the 1D Sn k-eigenvalue equations with multigroup approximation, written as:

$$\mu_\alpha \frac{\partial}{\partial x}\psi_{c,\alpha,g} + \sum\nolimits_{c,g}^{t}\psi_{c,\alpha,g} = \sum_{l=0}^{N_l} P_l(\mu_\alpha)\sum_{g'}^{N_g}\sum\nolimits_{c,g\leftarrow g',l}^{s}\phi_{c,g',l} + \frac{\chi_{c,g}}{k}\sum_{g'=1}^{N_g}\nu\sum\nolimits_{c,g'}^{f}\phi_{c,g',0} \quad (1)$$

Where

$\Psi_{c,\alpha,g}$ is the angular flux in cell c for group g in direction of angle a ;

μ_α is the cosine of the angle a ;

$\sum_{c,g}^{t}$ is the total cross section in cell c for group g ;

$\sum_{c,g\leftarrow g',l}^{s}$ is the lth order Legendre moment of the scattering cross section from g' to g in cell c ;

K is the eigenvalue ;

$\chi_{c,g}$ is the fission spectrum in cell c for group g;

$\sum_{c,g'}^{f}$ is the fission cross section in cell c for group g;

$P_l(\mu_\alpha)$ is the normalized Legendre polynomial of lth order evaluated at μ_α ;

N_l is the order of Legendre expansion;

N_g is the number of energy groups

And

$$\Phi_{c,g',l} = \sum_{a=1}^{N_a} w_a P_l(\mu_a)\psi_{c,a,g} \quad (2)$$

Where *Na* is the number of discrete angles. The weight corresponding to the discrete angle U_α is W_α for the chosen angular quadrature scheme.

Now, we divide the energy groups g into a number of coarse groups G such that each fine group belongs to one coarse group G as:

$$\mu_\alpha \frac{\partial}{\partial x}\psi_{c,\alpha,g} + \sum\nolimits_{c,g}^{t}\psi_{c,\alpha,g} = \sum_{l=0}^{N_l} P_l(\mu_\alpha)\sum_{G'}^{N_G}\sum_{g'\in G'}\sum\nolimits_{c,g\leftarrow g',l}^{s}\phi_{c,g',l} + \frac{\chi_{c,g}}{k}\sum_{G'}^{N_G}\sum_{g'\in G'}\nu\sum\nolimits_{c,g'}^{f}\phi_{c,g',0} \quad (3)$$

Now, we introduce a set of orthonormal basis vectors $P_i^G(g)$, where i is the order of the basis, G is the coarse group for the expansion. The Legendre polynomials have been used as the basis vectors in the original works. The basis vectors is from the performing proper orthogonal decomposition (POD) on snapshots, which will be presented in the following section in the present work.

$$\mu_\alpha \frac{\partial}{\partial x}\sum_{g\in G}P_i^G(g)\psi_{c,\alpha,g} + \sum_{g\in G}P_i^G(g)\sum\nolimits_{c,g}^{t}\psi_{c,\alpha,g} = \sum_{g\in G}P_i^G(g)\sum_{l=0}^{N_l}P_l(\mu_\alpha)\sum_{G'}^{N_G}\sum_{g'\in G'}\sum\nolimits_{c,g\leftarrow g',l}^{s}\phi_{c,g',l} + \frac{\chi_{c,g}}{k}\sum_{g\in G}P_i^G(g)\sum_{G'}^{N_G}\sum_{g'\in G'}\nu\sum\nolimits_{c,g'}^{f}\phi_{c,g',0} \quad (4)$$

In which, we define the flux moment as:

$$\phi_{c,G,i,l} = \sum_{g\in G}P_i^G(g)\phi_{c,g,l} \quad (5)$$

$$\psi_{c,a,G,i} = \sum_{g\in G}P_i^G(g)\psi_{c,\alpha,g} \quad (6)$$

Now, we can define the mapping relationship from fine group cross sections to the coarse group structure as:

$$\sum\nolimits_{c,G,0}^{t} = \frac{\sum_{g\in G}P_0^G\sum_{c,t}^{g}\phi_{c,g,0}}{\sum_{g\in G}P_0^G(g)\phi_{c,g,0}} \quad (7)$$

$$\delta_{c,a,G,i} = \frac{\sum_{g\in G}P_i^G(g)(\sum_{c,g}^{t}-\sum_{c,G,0}^{t})\psi_{c,a,g}}{\sum_{g\in G}P_0^G(g)\psi_{c,a,g}} \quad (8)$$

$$\sum\nolimits_{c,G\leftarrow G',i,l}^{s} = \frac{\sum_{g'\in G'}P_0^G(g)\sum_{c,g\leftarrow g',l}^{s}\phi_{c,g',l}}{\sum_{g'\in G'}P_0^G(g)\phi_{c,g',l}} \quad (9)$$

$$\nu\sum\nolimits_{c,G}^{f} = \frac{\sum_{g\in G}P_0^G(g)\nu\sum_{c,g}^{f}\phi_{c,g,0}}{\sum_{g\in G}P_0^G(g)\phi_{c,g,0}} \quad (10)$$

$$\chi_{c,G,i} = \sum_{g\in G}P_i^G(g)\chi_{c,g} \quad (11)$$

Combine the definitions in Eq.(6) and (8) yelids:

$$\sum\nolimits_{c,G,0}^{t}\psi_{c,a,G,i} + \delta_{c,a,G,i}\psi_{c,a,G,0} = \sum_{g\in G}P_i^G(g)\sum\nolimits_{c,G}^{t}\psi_{c,\alpha,g} \quad (12)$$

Eqs. (9)–(12) are substituted into Eq. (4) with Eq. (6) to yield, and split the total cross section to two components $\sum_{c,G,0}^{t}$ and $\delta_{c,a,G,i}$, which represent the scalar and angular dependent components.

$$\mu_\alpha \frac{\partial}{\partial x}\psi_{c,a,G,i} + \sum_{c,G,0}^{t}\psi_{c,a,G,i} + \delta_{c,a,G,i}\psi_{c,a,G,0} = \sum_{l=0}^{N_l} P_l(\mu_\alpha) \sum_{G'=1}^{N_G} \sum_{c,G\leftarrow G',i,l}^{s} \phi_{c,G',0,l} + \frac{\chi_{c,G,i}}{k} \sum_{G'=1}^{N_G} \nu \sum_{c,G'}^{f} \phi_{c,G',0,0} \quad (13)$$

In Eq(13), the term $\delta_{c,a,G,i}$ represents the correction to isotropic total cross section.

2.2 Proper orthogonal decomposition

The previous work has shown that the common mathematical orthogonal basis functions needs the higher degrees of freedom to approximate the fine group flux. We seek a form of basis functions which utilize proper orthogonal decomposition) to incorporate spectral snapshots to generate. The central goal of POD is to generate an orthogonal basis expansion with a truncated order N that minimizes the least squares error with the target function *f(x)*. In some applications, such as image compression, the function f is predetermined, e.g., a set of pixel values. For other applications, such as reduced order modeling, the function f is not known. Snapshots is a method used to generate the POD basis [10]. In this work, we regard the fine group flux as the snapshot, which is a priori unknown. Hence, selecting appropriate snapshots is also a crucial task in this work. The energy-dependent flux within a spatial cell of the representative (test) problem is a snapshot denoted by the vector dn. These vectors form the columns of the matrix $D \in R^{M*N}$, where *M* is the number of energy-groups, and *N* is the number of snapshots. The basis is formed by first defining the matrix $B = D^T D$, which is semi-positive definite. Alternatively, the method could proceed using *D* instead of *B* as the methods are equivalent, but a semipositive definite matrix simplifies much of the linear algebra.

We perform the SVD on the matrix *B*, which is equivalent to the eigen-decomposition for semi-positive definite matrices as:

$$B = U_B \sum_B V_B^T = Q \wedge Q^{-1} \quad (14)$$

where $U_B \in R^{N*N}$ and $V_B \in R^{N*N}$ are unitary and contain the left andright singular vectors, respectively. The matrix $\sum_B \in R^{N*N}$ is a diagonal matrix containing the singular values. The matrix $Q \in R^{N*N}$ is unitary and contains the eigenvectors of *B* with corresponding eigenvalues contained in the diagonal matrix $\Lambda \in R^{N*N}$.

Since the matrix *B* is semi-positive definite, $U_B = V_B = Q = V_D$ are the right singular vectors of *D*, and $\Lambda_B = \sum_B = \sum_D^2$ are the square of the singular values of *D*, i.e.,

$$D^T D = V_D \sum_B U_D^T U_D \sum_D V_D^T = V_D \sum_D^2 V_D^T = Q \wedge Q \quad (15)$$

To form the POD basis, first we arrange the singular values and corresponding vectors in decreasing order, which sets the zeroth order basis as the most fundamental mode within the snapshots. Now, project the snapshots onto the modes as:

$$\boldsymbol{p}_j = D\boldsymbol{q}_j \quad (16)$$

Alternatively, expressed in matrix form:

$$P = DQ \quad (17)$$

An arbitrary length M vector f may be approximately represented as:

$$f \approx \sum_{j=0}^{k} a_j \boldsymbol{p}_j \quad (18)$$

The POD basis creates the set of length M basis vectors which provide the best kth order expansion in the least squares sense as long as the snapshots closely approximate the function f. If $N \geq M$ then the basis *P* is complete and any length *M* vector can be reproduced exactly using the first *M* vectors of *P*.

Since the DGM method requires a flat zeroth order basis as previously mentioned, such a vector is inserted as p0, and the remaining columns are shifted by one. The vector corresponding to the smallest eigenvalue is discarded, and the matrix *P* is reorthonormalized. This work will explore how closely the snapshots must approximate the fluxes to provide an adequate basis for the DGM method when using truncated basis sets.

3.method

3.1 DGM algorithm

In order to assess the effectiveness and efficiency of the POD-based DGM method, in this study, we extended the development of the 1-D discrete ordinates code, originally developed by Richard Reed. The same 16-angle Gauss Legendre quadrature and the diamond-difference approximation were employed in this work. The code follows the recondensation algorithm employed in previous work and the Krasnoselskii iteration[1]. The core formula of this iterative format can be represented as follows:

$$x^{(n+1)} = (1-\lambda)x^n + \lambda A x^n \quad (19)$$

Notice that if k is set to unity, Krasnoselskii iteration reduces to Picard iteration. Eq. (19) is used in the DGM algorithm to compute the fine-group flux used in the next recondensation iteration. By adjusting the value of λ, one may select for higher computational expense in exchange for stability. Thus there exists an optimum value for k, which cannot be known a priori, which produces a stable (convergent) progression with the

least computational work. It was found that a (non-optimum) value. In our study, a uniform value of λ=0.8 was employed for the sake of computational stability.

Building upon the previous work, the core logic of the code has been established. According to the eq 11 mentioned earlier, the moments of the fission spectrum do not depend on the reconstructed energy group flux, which can be observed that before the iteration process. In the iteration process, the moments of cross-sections can be calculated using the current iterative orthogonal basis and fine-group flux. This is followed by using the transport solver to solve for the zeroth-order flux moment and eigenvalue, as described in equation (13). Finally, with the obtained moments, the source terms of higher-order moments are solved as per the zeroth-order solution. Once all the moments are obtained for the current state, the fine-group flux can be updated using the orthogonal basis. The process iterates, updating cross-section moments in each iteration until convergence criteria are met. The DGM computation process is illustrated in Algorithm 1. As shown below:

Algorithm 1: Recondensation algorithm for the DGM method

```
Input: mesh, material, basis functions
Result: updated flux, coarse group sections
Calculate χ and Q moments
Initial fine group flux
While not converged do
    Compute flux moments
    Compute cross section moments
    Solve the order 0 equation
    Update eigenvalue
    For the moment in order=i>0 do
        Solve ith-order equation
    End
    Reconstruct the fine group flux
End
```

3.2 Selecting Coarse group structure

Another distinction between the DGM method and traditional group condensation methods is that its coarse-group structure selection doesn't follow the current conventional general coarse-group structures. Instead, it's based on a set of specific group-collapsing constraints, ensuring the stability and efficiency of the DGM method. Previous work[1] suggested guidelines for selecting an appropriate structure that allows higher values of k for use in Krasnoselskii iteration. The guidelines used in this work are:

- Limit ratio of smallest to largest Σ_t within coarse-group, where Σ_t has been averaged over the fuel materials
- Relax ratio condition for coarse-groups with small Σ_t
- Limit the number of fine-groups per coarse-group
- Force coarse-group breaks where desired

In this work, due to the test problem with different energy spectrum and energy group structure. the Scale 44- and 238-group structures were considered to esting the applicability of this method.

4 Test problem

In this study, we tested two problems. One is the commonly used 1D repeating 44-group UO2 and MOX 10-pin problem for testing the DGM method program shown in figure1 for testing the code and the snapshot choice method. There are 22 fuel mesh and water in every cell for this problem. The other is the more complex 1D 238-group HTTR problem with a more intricate energy spectrum shown in figure2 to optimize the efficiency of the DGM method[11]. The mesh discretization for this problem is more complex than the 10-pin case. Please refer to Table 1 for specific details.

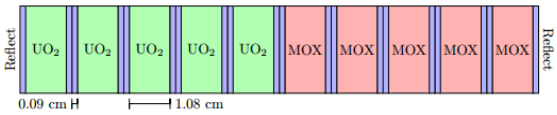

Fig.1. Depiction of the 10-pin problem

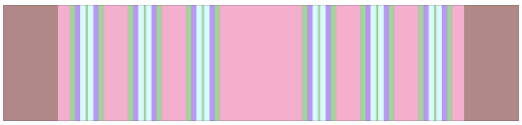

Fig.2. Depiction of the HTTR problem

Tab.1 Depiction of the detail in HTTR problem

Geometry		Material		
Width	Mesh number	Graphite reflector	Fuel	Center graphite
0.9046	5	Graphite+B4C	Graphite	Graphite
0.3819	2	Graphite+B4C	He Gas	Graphite
0.3492	2	Graphite+B4C	Sleeve	Graphite
0.4190	2	Graphite+B4C	Fuel	Graphite
0.1455	1	Graphite+B4C	He Gas	Graphite
0.4190	2	Graphite+B4C	Fuel	Graphite
0.3492	2	Graphite+B4C	Sleeve	Graphite
0.3819	2	Graphite+B4C	He Gas	Graphite
0.9046	5	Graphite+B4C	Graphite	Graphite

As discussed previously, the POD basis requires a number of spectral snapshots with which to construct the orthogonal basis. The best snapshots would be from the full spectral shape for the complete problem, and these were used to create the ‘‘full” basis in both problem. In practical applications, these snapshots would be unavailable as the solution to the problem is required to solve the problem. However, the full snapshots provide insight into the best performing POD basis functions, thus are used as a comparison in this work

5 result

5.1 10-pin problem

The small representative snapshot is created to replace the full problem snapshot, which include: infinite pins of UO2 pins with reflective boundary, infinite pins of MOX pins with reflective boundary, the juntion of the above two pins, a UO2 pin adjacent to a MOX pin that includes the interference in the combine. These snapshots are respectively referred to as "UO2"," MOX", "junction", "combine". The cross section of these snapshots are predefined in the continuous Monte Carlo code SERPENT[12]. then with our SN code to obtain the fine group energy spectrum.

In this problem, the ratio of smallest to largest cross section was set to 1.3. This atio was ignored if the largest total cross section within the coarse group was below1.0 cm^{-1}. Finally, a maximum of 60 fine groups were allowed within each coarse group. The mapping between coarse group and fine group is shown in Table 2 as follows:

Tab.2. The mapping relationship of 10-pin problem

CG	FG
0	1 ~ 26
1	27 ~ 41
2	42 ~ 43
3	44

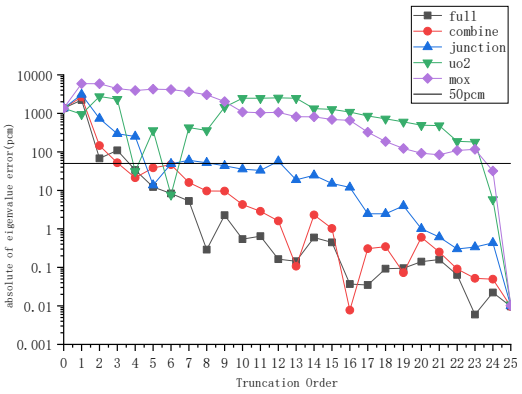

Fig.3 Eigenvalue of 10-pin problem with different truncation orders

The eigenvalue of this problem in different truncation orders is shown in Figure3. With 50 pcm error as reference, the full basis can stably converge within this range at 4th order. However, since this basis cannot be obtained in advance, the best performance is observed with the combine basis, which can achieve an eigenvalue deviation within 50 pcm at 7th order, specifically 37 pcm. Following this, the junction basis stabilizes within 50 pcm deviation at 9th order, at 49 pcm. Both of them are generated from snapshots containing complete lattice information. The combine basis, due to obtaining the information about interference between lattice, performs better. On the other hand, the UO2-basis and MOX-basis, containing relatively incomplete physical information, exhibit relatively poorer performance, only showing better eigenvalue deviation results in the full order, which is similar to the DLPs basis.

The energy spectrum of different basis in 5th order is shown in Figure4. Due to the presence of negative fluxes at low truncation orders, in this study, to standardize this process, an absolute value operation was applied to the final accumulated energy spectra. The Figure5 is the energy spectrum deviations of different basises with 44-group SN transport calculation result. The absolute value operation was also applied to the deviations.

To further analyze the accuracy of the combine basis in energy spectrum reconstruction, a comparison was conducted for the deviations between the energy spectrum of UO2-pin, the MOX-pin through reconstruction and reflective boundary calculation with the most obvious interference and the two pins' energy spectrum obtained from 44-group fine-group calculations. These comparisons are illustrated in Figures 6 and 7, respectively.

For the test problem, using the combine basis, effective reconstruction of the energy spectrum of the test problem can be achieved at the 7th order, with flux deviations for each fine energy group being less than 0.3%. For the energy spectrum reconstruction of the UO2 and MOX lattice, where spatial interference is most evident, the flux deviations for each energy group remain below 0.5% at the 7th order. Compared to the performance of the POD parallel-group method, the zeroth-order spectrum, i.e., the traditional parallel-group method's spectrum, compared to the fine-group spectrum, has an average flux deviation of more than 14% even in the best-performing 1st group at fewer groups.

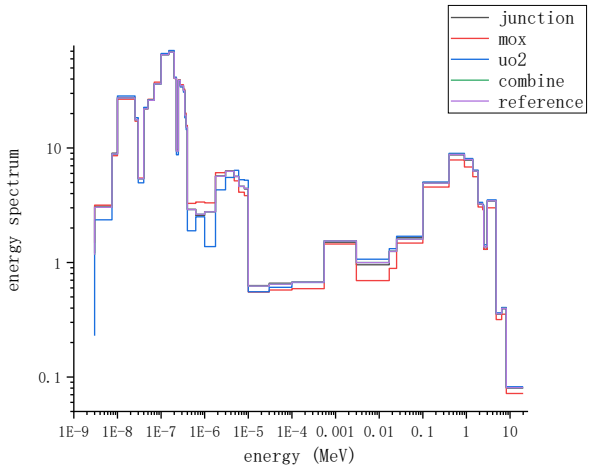

Fig.4. the energy spectrum of different basis in 5th order for 10-pin problem

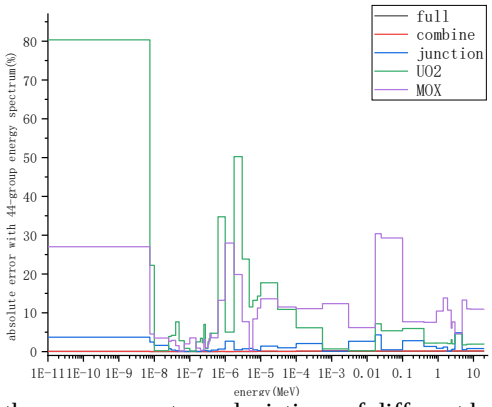

Fig.5. the energy spectrum deviations of different basis in 5th order for 10-pin problem

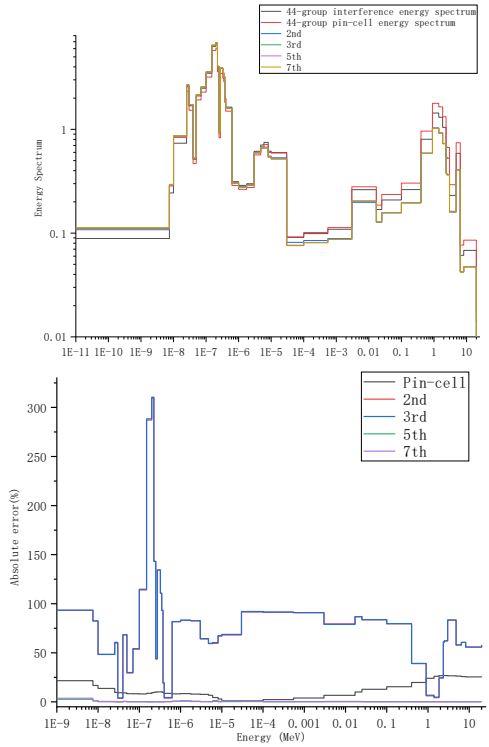

Fig.6. the energy spectrum and deviations of different order for combine-UO2 pin

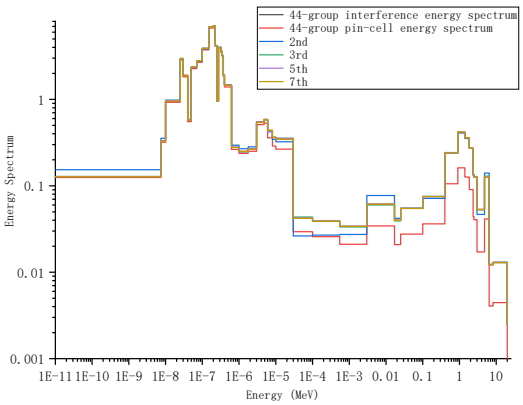

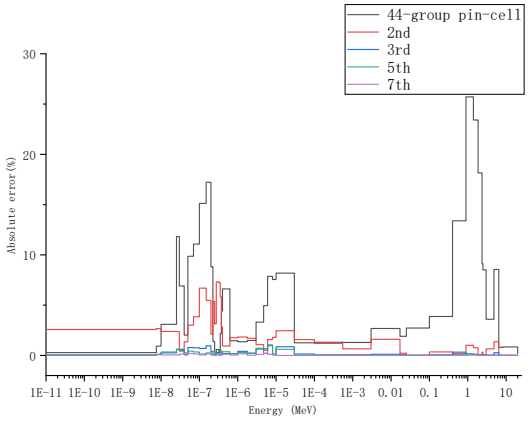

Fig.7. the energy spectrum and deviations of different order for combine-MOX pin

5.2 HTTR Problem

The 10-pin problem have demonstrated the functionality of our program and the general principle of snapshot selection, which is to preserve as much of the physical information within the problem as possible. We selected the more complex HTTR problem to further investigate the applicability and efficiency of the POD-based DGM method. Based on the general principle, we just take study to the combine basis and full basis. The combine basis is from a snapshot developed by a graphite reflector pin, two fuel pins and a center graphite pin.

In this problem, the ratio of smallest to largest cross section was set to 1.2. This ratio was ignored if the largest total cross section within the coarse group was below1.2 cm-1. Finally, a maximum of 30 fine groups were allowed within each coarse group. The mapping between coarse group and fine group is shown in Table 3.

The Table 4 shows the eigenvalue and error with fine-group SN result. With 50 pcm error as reference, the combine basis only requires a higher order than the full basis. The figure 8 and 9 show the reconstructed energy spectrum in different truncation order and the deviations with fine group energy spectrum. There are significant deviations in the energy groups with the lowest and highest energies. This is primarily due to the low flux in these energy groups, resulting in more negative flux values in SN calculation. After applying the absolute value operation, these deviations become prominent. However, since neutron flux is low in these groups, the overall impact is not substantial. The effective convergence of eigenvalues with truncation order provides strong evidence for the DGM's efficacy despite these deviations.

Table 3 mapping relations between coarse groups and fine groups

CG	FG
0	1-16
1	17-46
2	47-76
3	77-106
4	107-136
5	137
6	138-147
7	148-177
8	178-207
9	208-237
10	238

From these results, it can be observed that the performance of the combine basis closely aligns with full basis in terms of energy spectrum reconstruction for most fine groups. The overall eigenvalue deviations are also quite similar. This basis can be considered to represent the most effective outcome achievable with the POD-based DGM method in the HTTR problem. Examining the performance of the combine basis at different truncation orders reveals that at the 3rd order, neutron flux deviations for most energy groups are around 1%, while at the 4th order, deviations for most energy groups can be maintained at around 0.1%. Furthermore, the eigenvalue error can be controlled within 30 pcm at this order.

Table 4 the eigenvalue and error of two kinds of basis in HTTR problem

Order	Full basis		Combine basis	
	k_{eff}	Error/pcm	k_{eff}	Error/pcm
0	0.951815	-9676.1	0.951815	-9676.1
1	1.034203	-1437.3	1.038287	-1028.9
2	1.046499	-207.7	1.048685	10.8
3	1.048553	-2.3	1.049694	111.8
4	1.048547	-2.9	1.048327	-24.9
5	1.048580	0.3	1.048558	-1.8
6	1.048573	-0.3	1.048566	-1.0

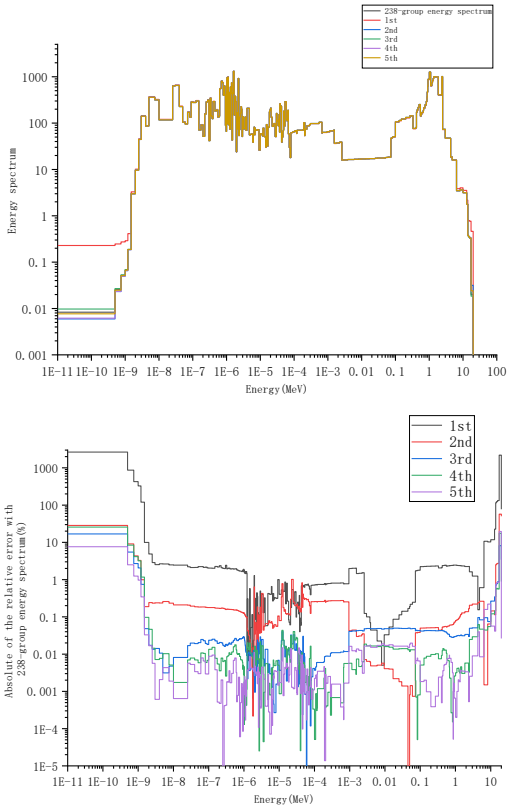

Fig.8. the energy spectrum deviations of full basis in different orders for HTTR problem

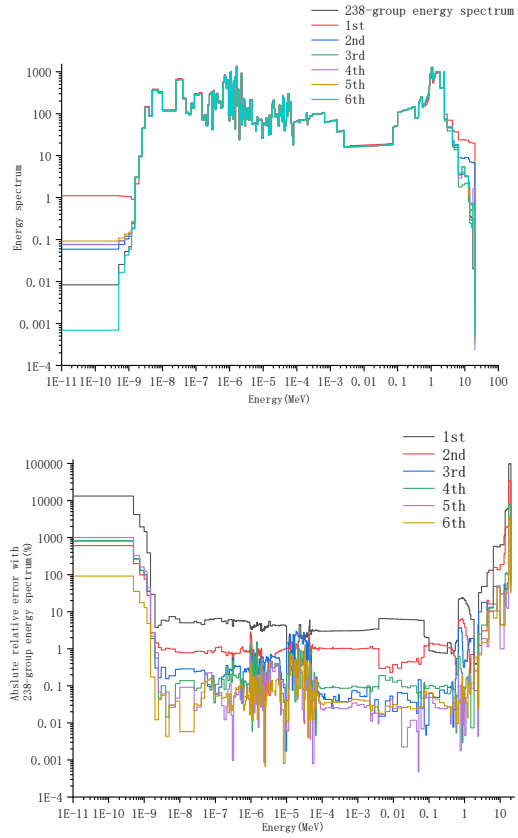

Fig.9. the energy spectrum deviations of combine basis in different orders for HTTR problem

5.3 Efficiency test

The DGM method has effectively reconstructed the fine-group energy spectrum, making it possible to obtain homogenized cross-sections for coarse-group collapsing, but there are certain efficiency issues. For the HTTR problem, the computation time required for truncation up to the fourth order has become almost equivalent to fine-group SN transport calculations and even consumes more memory. Due to it, we have take research on its convergence process and relaxed convergence criteria to achieve higher.

Figure 10 is iteration parameters change with reconstruction times in 10-pin problem with 3rd order with combine basis. This process is representative in which it's evident that the eigenvalues have become relatively stable after 50 iterations of reconstruction.

Based on this situation, we test the method of calculation time through control ing the reconstruction times in every order in HTTR problem. The eigenvalue result and the radio of reconstruction time to the fine group transport calculation time of different truncation orders with combine basis is shown in Table 5. The energy spectrum and deviation of different truncation orders with combine basis is shown in Figure 10.

Table 5 the eigenvalue and error of combine basis in HTTR problem with teration times=50

Order	Eigenvalue	Error（pcm）	Time radio （%）
1	1.021815865	-2676.425898	3.89
2	1.041428935	-715.1188671	9.26
3	1.052283352	370.3228203	15.83
4	1.049134582	55.44584828	22.13
5	1.048065808	-51.43161532	28.16
6	1.048196856	-38.32677004	34.98
7	1.047954259	-62.58652632	40.56

From Table 5 and Figure 10, it can be observed that by controlling iteration times, although the error increases compared to full convergence, effective control over computational time has been achieved, making the DGM method a truly viable approach for group collapsing.

6 Conclusion

In this article, we conducted a study on the DGM method based on POD. We developed a 1D DGM computational program and tested it for snapshot selection and group-collapsing constraints. We achieved accurate energy spectrum reconstruction for 1D 10-pin UO2-MOX problems and the HTTR problem. Furthermore, we investigate the efficiency of the DGM method and successfully reduced computational time by controlling reconstruction iteration times, with a slight increase in calculation error. This research demonstrates the promising potential of the POD-based DGM method. In the future, we will continue to explore its efficiency and applicability in two-dimensional problems.

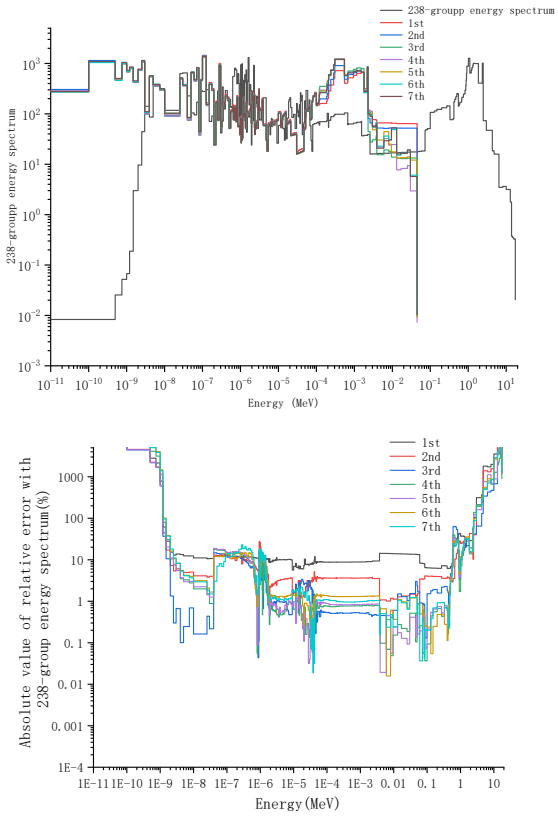

Fig.10. the energy spectrum deviations of combine basis with iteration times=50 in different orders for HTTR problem

REFERENCES

[1] GIBSON N A, FORGET B. On the stability of the discrete generalized multi-group method[J]. Annals of Nuclear Energy, 2014, 65: 421-432.

[2] Yang W, Wu HC, Li YZ. Development and Verification of a PWR Pin-by-pin Core Analysis Code[C]. Proceedings of the Reactor Physics Asia 2017 (RPHA17) Conference, Chengdu, China, Aug. 24-25, 2017.

[3] RAHNEMA F, DOUGLASS S, FORGET B. Generalized energy condensation theory[J]. Nuclear Science and Engineering, 2008, 160(1): 41-58.

[4] Zhu, L., Forget, B., 2010. A discrete generalized multigroup energy expansion theory. Nuclear. Sci. Eng. 166 (3), 239–253.

[5] Zhu, L., Forget, B., 2011. An energy recondensation method using the discrete generalized multigroup energy expansion theory. Annals of Nuclear Energy 38 (8), 1718–1727.

[6] Douglass, S., Rahnema, F., 2012. Consistent generalized energy condensation theory. Annals of Nuclear Energy 40 (1), 200–214.

[7] REED R L, ROBERTS J A. Effectiveness of the discrete generalized multigroup method based on truncated, POD-driven basis sets[J]. Annals of Nuclear Energy, 2019, 126: 253-261.

[8] REED R L, ROBERTS J A. An energy basis for response matrix methods based on the Karhunen-Loéve transform[J]. Annals of Nuclear Energy, 2015, 78: 70-80.
[9] REED R L, ROBERTS J A. Application of the Karhunen-Loève transform to the C5G7 benchmark in the response matrix method[J]. Annals of Nuclear Energy, 2017, 103: 350-355.
[10] Buchan, A.G., Pain, C.C., Fang, F., Navon, I.M., 2013. A pod reduced-order model for eigenvalue problems with application to reactor physics. Int. J. Numer. Meth. Eng. 95 (12), 1011–1032.
[11] Douglass S, Rahnema F. Specification for a 1-dimensional gas-cooled reactor benchmark problem for neutron transport[J]. Transactions of the American Nuclear Society, 2011, 104: 74.
[12] Leppänen, J., Pusa, M., Viitanen, T., Valtavirta, V., Kaltiaisenaho, T., 2014. The serpent monte carlo code: Status, development and applications in 2013, 06021.